9

On the Analysis and Kinematic Design of a Novel 2-DOF Translational Parallel Robot

Jinsong Wang, Xin-Jun Liu and Chao Wu

1. Introduction

The conceptual design of parallel robots can be dated back to the time when Gough established the basic principles of a device with a closed-loop kinematic structure (Gough 1956), that can generate specified position and orientation of a moving platform so as to test tire wear and tear. Based on this principle, Stewart designed a platform for use as an aircraft simulator in 1965 (Stewart 1965). In 1978, Hunt (1978) made a systematic study of robots with parallel kinematics, in which the planar 3-RPS (R-revolute joint, P-prismatic joint, and S-spherical joint) parallel robot is a typical one. Since then, parallel robots have been studied extensively by numerous researchers.

The most studied parallel robots are with 6 DOFs. These parallel robots possess the advantages of high stiffness, low inertia, and large payload capacity. However, they suffer the problems of relatively small useful workspace and design difficulties (Merlet 2000). Furthermore, their direct kinematics possess a very difficult problem; however the same problem of parallel robots with 2 and 3 DOFs can be described in a closed form (Liu 2001). As is well known, there are three kinds of singularities in parallel robots (Gosselin and Angeles 1990). Moreover, not all singularities of a 6-DOF parallel robot can be found easily. But for a parallel robot with 2 and 3 DOFs, the singularities can always be identified readily. For such reasons, parallel robots with less than 6 DOFs, especially 2 and 3 DOFs, have increasingly attracted more and more researchers' attention with respect to industrial applications (Tsai & Stamper 1996; Ceccarelli 1997; Tonshoff et al 1999; Siciliano 1999; Liu et al. 2001; Liu et al. 2005; Liu & Kim 2003). In these designs, parallel robots with three translational DOFs have been playing important roles in the industrial applications (Tsai & Stamper 1996; Clavel 1988; Hervé 1992; Kim & Tsai 2002; Zhao & Huang 2000; Carricato & Parenti-Castelli 2001; Kong & Gosselin 2002; Liu et al. 2003), especially, the DELTA robot (Clavel 1988), which is evident from the fact that the design of the DELTA robot is covered by a family of 36 patents (Bonev 2001). Tsai's robot (Tsai & Stamper 1996), in which each of the three legs consists of a parallelogram, is the first design to solve the problem of UU chain. A 3-

Source: Industrial-Robotics-Theory-Modelling-Control, ISBN 3-86611-285-8, pp. 964, ARS/plV, Germany, December 2006, Edited by: Sam Cubero

translational-DOF parallel robot, Star, was designed by Hervé based on group theory (Hervé 1992). Such parallel robots have wide applications in the industrial world, e.g., pick-and-place application, parallel kinematic machines, and medical devices.

The most famous planar 2-DOF parallel robots (Asada & Kanade 1983; McCloy 1990; Gao et al. 1998) are the well-known five-bar mechanism with prismatic actuators or revolute actuators. In the case of the robot with revolute actuators, the mechanism consists of five revolute pairs and the two joints fixed to the base are actuated. In the case of the robot with prismatic actuators, the mechanism consists of three revolute pairs and two prismatic joints, in which the prismatic joints are usually actuated. The output of the robot is the translational motion of a point on the end-effector, i.e., the orientation of the end-effector is also changed correspondingly. Accordingly, some versions of the 2-DOF translational parallel robot (TPR) have been disclosed. One of them has been applied in precise pick & place operations at high speed in IWF at Technical University of Braunschweig. In 2001, another 2-DOF TPR has been proposed for the conceptual design of a 5-axis machine tool (Liu 2001). The structure, kinematics and dynamics of the TPR were discussed in details (Liu et al., 2002; Liu et al., 2005). Recently, a 2-DOF TPR with revolute actuators was introduced (see Table 1 in (Liu & Wang, 2003); Huang et al., 2004). The TPR presented in (Liu 2001; Liu et al., 2005) has been used in the design of a planer machine tool with a gantry structure instead of a traditional one with serial chains to improve its stiffness and inertia characteristics. However, all of these TPRs consist of at least of one parallelogram. Here, a novel 2-DOF TPR with only revolute and prismatic joints will be proposed. The robot can position an objective with constant orientation with high speed.

As it is one of the most important and challenging issues in the parallel robot, optimal kinematic design has drawn more and more researchers' attention (Gosselin & Angeles, 1989; Chablat & Wenger, 2003; Stock & Miller, 2004; Ottaviano & Ceccarelli, 2002; Cervantes-Sánchez et al., 2001). The objective of optimal kinematic design is determining the dimension or link length of a robot with respect to desired performance(s). Due to the parameter infinity and the instability of performance in a whole workspace, optimal kinematic design is one of the most challenging problems in the field of parallel robot. The commonly used methods are first to develop an objective function and then to reach the result using the numerical method with an algorithm. These methodologies have the disadvantages in common, i.e., the objective function is difficult to be established; the numerical procedure may lead to a solution that is quite far away from the optimal solution; the process is iterative and time consuming; and, most fatally, only one optimal solution can be provided. To overcome the disadvantages, in this chapter, a new optimal design methodology will be proposed for the parallel robot. Using a normalization method, the dimensional characteristic parameters of the robot will be normalized. The nor-

malization can guarantee that a dimensional robot and its corresponding normalized robot are similar not only in size but also in performance. The dimensional robot is defined as *similarity robot* (SR), and the normalized robot is referred to as *basic similarity robot* (BSR). A design space which embodies all kinds of BSRs will be established. The space can be used not only in analysis but also in the optimal design of the parallel robot. Within the design space, the performance atlas that illustrates the relationship between a performance index and the BSRs can be plotted. The optimal kinematic design can be implemented with respect to the performance atlases. Design examples will be finally given in the chapter. Compared with the traditional design methods, the proposed optimal design methodology has some advantages as follows: (a) one performance index corresponds to one atlas; (b) for such a reason in (a), the fact that some performance indices are antagonistic is no longer a problem in the design; (c) the optimal design process can consider multi-objective functions or multi-indices, and also guarantees the optimal result; and finally, (d) the design method provides a set of possible solutions, and ideally, all the design solutions.

2. Description of the 2-DOF TPR and its Topological Architectures

2.1 Architecture description

The novel 2-DOF translational parallel robot proposed here is shown in Fig. 1(a). A schematic of the robot is shown in Fig. 1(b). The end-effector of the robot is connected to the base by two kinematic legs 1 and 2. Leg 1 consists of three revolute joints and leg 2 two revolute joints and one cylinder joint, or three revolute joints and one prismatic joint. In each leg, the revolute joints are parallel to each other. The axes of the revolute joints in leg 1 are normal to those of the joints in leg 2. The two joints attached to the end-effector are put in the adjacent sides of a square. The kinematic chain of the robot is denoted as RRR-RRC (C-cylinder joint) or RRR-RRRP.

2.2 Capability

Here, a Plücker coordinate like $\$_j=(\bar{x}, \bar{y}, \bar{z}; \hat{x}, \hat{y}, \hat{z})$ is used to describe the capability of an object j. In $\$_j$, $Tr_j=(\bar{x}, \bar{y}, \bar{z})$ and $Ro_j=(\hat{x}, \hat{y}, \hat{z})$ express the translation and rotation of the object, respectively. If an element in $\$$ is equal to 0, there is no such a translation or rotation. If it is equal to 1, there is the capability. For example, $\bar{x}=0$ means that the object has no the translation along the x-axis; $\hat{y}=1$ indicates that the object can rotate about the y-axis.

Observing only the leg 1, the Plücker coordinate of the end-effector in the leg can be written as $\$_1$=(1, 1, 0; 0, 0, 1). Letting the leg 1 alone, the Plücker coordinate of the end-effector with the leg 2 can be expressed as $\$_2$=(1, 1, 1; 1, 0, 0). Then, the intersection of the two Plücker coordinates $\$_1$ and $\$_2$ is $\$, i.e.,

$$\$=\$_1 \cap \$_1=(1, 1, 0; 0, 0, 1) \cap (1, 1, 1; 1, 0, 0)= (1, 1, 0; 0, 0, 0) \quad (1)$$

which describes the capability of the robot, i.e., the translations of the end-effector along the x and y axes. That means the end-effector has two purely translational degrees of freedom with respect to the base.

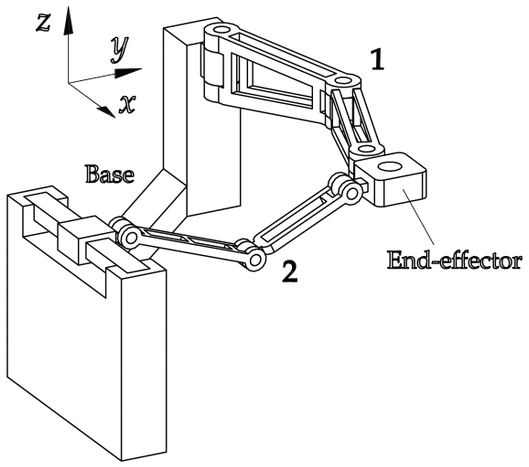

(a)

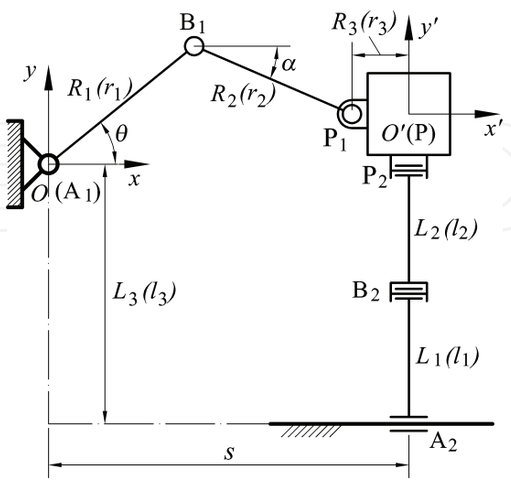

(b)

Figure 1. The 2-DOF translational parallel robot: (a) the CAD model; (b) the schematic

2.3 Topological architectures

Observing the robot shown in Fig. 1, it is not difficult to reach such a conclusion that if the axes of the joints in the leg 1 are normal to those of the joints in the leg 2 the robot will have two translational DOFs. Based on this idea, some topological architectures are shown in Fig. 2. It is noteworthy that the leg 2 shown in Fig. 1 and Fig. 2 can be also the kinematic chain RRR(Pa) shown in Fig. 3, where Pa means planar parallelogram.

3. Kinematics Analysis

Although the robot has some topologies, this chapter consideres only the architecture shown in Fig. 1. In this section, the inverse and forward kinematics of the robot will be given.

3.1 Inverse kinematics

As illustrated in Fig. 1(b), a reference frame $\Re : O - xy$ is fixed to the base at the joint point A_1 and a moving reference frame $\Re' : O' - x'y'$ is attached to the end-effector, where O' is the reference point on the end-effector. Vectors $\boldsymbol{p}_{i\Re}$ $(i = 1, 2)$ will be defined as the position vectors of points P_i in frames $\Re$, and vectors $\boldsymbol{b}_{i\Re}$ $(i = 1, 2)$ as the position vectors of points B_i in frame $\Re$. The geometric parameters of the robot are $A_1B_1 = R_1(r_1)$, $B_1P_1 = R_2(r_2)$, $PP_i = R_3(r_3)$, $A_2B_2 = L_1(l_1)$, $B_2P_2 = L_2(l_2)$, and the distance between the point A_1 and the guideway is $L_3(l_3)$, where R_n and L_n (n=1,2,3) are dimensional parameters, and r_n and l_n non-dimensional parameters. The position of point O' in the fixed frame $\Re$ is denoted as vector

$$\boldsymbol{c}_{\Re} = (x, \quad y)^{\mathrm{T}} \tag{2}$$

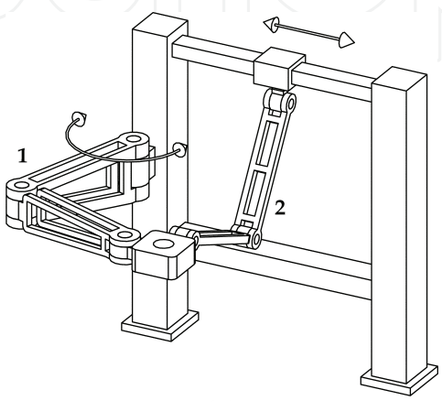

(a)

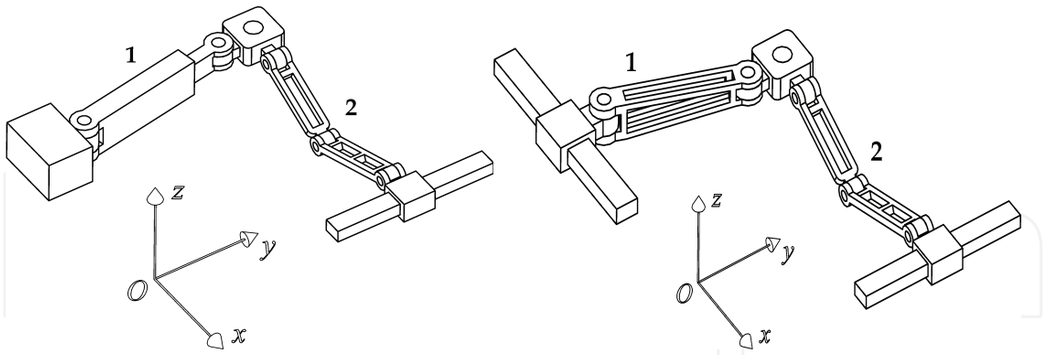

(b) (c)

Figure 2. Some topological architectures: (a) RRR-RRRP chain (arrangement is different from that shown in Fig. 1); (b) RPR-RRRP chain; (c) PRR-RRRP chain.

The vectors of $\boldsymbol{b}_{1\Re}$ in the fixed frame $\Re$ can be written as

$$\boldsymbol{b}_{1\Re} = \begin{pmatrix} R_1 \cos\theta & R_1 \sin\theta \end{pmatrix}^{\mathrm{T}} \tag{3}$$

where θ is the actuated input for the leg 1. Vector $\boldsymbol{p}_{1\Re}$ in the fixed frame $\Re$ can be written as

$$\boldsymbol{p}_{1\Re} = \begin{pmatrix} -R_3 & 0 \end{pmatrix}^{\mathrm{T}} + \boldsymbol{c}_{\Re} = \begin{pmatrix} x - R_3 & y \end{pmatrix}^{\mathrm{T}} \tag{4}$$

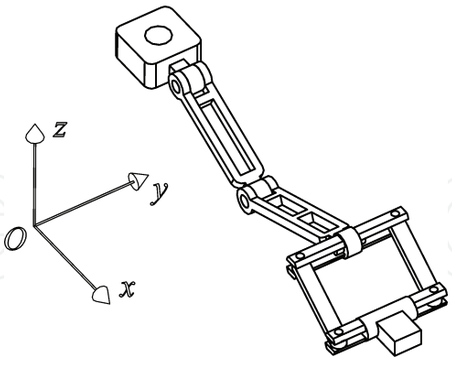

Figure 3. One topological architecture of the leg 2

The inverse kinematics problem of the leg 1 can be solved by writing following constraint equation

$$\left\| \boldsymbol{p}_{1\Re} - \boldsymbol{b}_{1\Re} \right\| = R_2 \tag{5}$$

that is

$$(x - R_3 - R_1\cos\theta)^2 + (y - R_1\sin\theta)^2 = R_2^2 \tag{6}$$

Then, there is

$$\theta = 2\tan^{-1}(m) \tag{7}$$

where

$$m = \frac{-b + \sigma\sqrt{b^2 - 4ac}}{2a} \tag{8}$$

$\sigma = 1$ or -1

$a = (x - R_3)^2 + y^2 + R_1^2 - R_2^2 + 2(x - R_3)R_1$

$b = -4yR_1$

$c = (x - R_3)^2 + y^2 + R_1^2 - R_2^2 - 2(x - R_3)R_1$

For the leg 2, it is obvious that

$$s = x \tag{9}$$

in which s is the input of the leg 2. From Eqs. (8) and (9), we can see that there are two solutions for the inverse kinematics of the robot. Hence, for a given robot and for prescribed values of the position of the end-effector, the required actuated inputs can be directly computed from Eqs. (7) and (9). To obtain the configuration as shown in Fig.1, parameter σ in Eq. (8) should be 1. This configuration is called the "+" working mode. When $\sigma = -1$, the corresponding configuration is referred to as the "—" working mode.

3.2 Forward kinematics

The forward kinematic problem is to obtain the output with respect to a set of given inputs. From Eqs. (6) and (9),one obtains

$$y = e + \sigma\sqrt{f} \tag{11}$$

and

$$x = s \tag{12}$$

where, $e = R_1\sin\theta$ and $f = R_2^2 - (s - R_3 - R_1\cos\theta)^2$. Therefore, there are also two forward kinematic solutions for the robot. The parameter $\sigma = -1$ corre-

sponds to the configuration shown in Fig. 1, which is denoted as the *down-configuration*. When $\sigma = 1$, the configuration is referred to as the *up-configuration*. These two kinds of configurations correspond to two kinds of assembly modes of the robot.

Figure 4 illustrates two kinds of working modes of the robot. The two kinds of assembly modes are shown in Fig. 5. In this chapter, the robot with both the "+" working mode and *down-configuration* will be considered only.

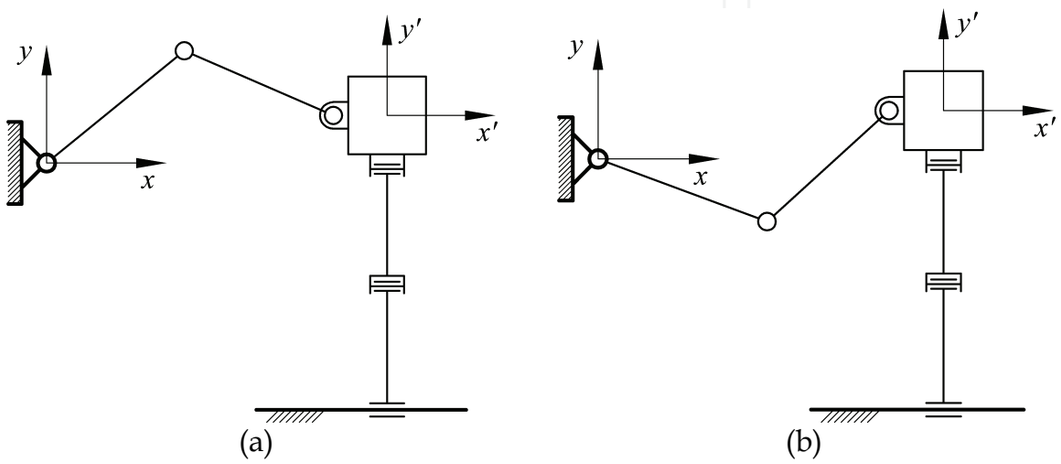

Figure 4. Two kinds of working modes: (a) "+" working mode; (b) "—" working mode

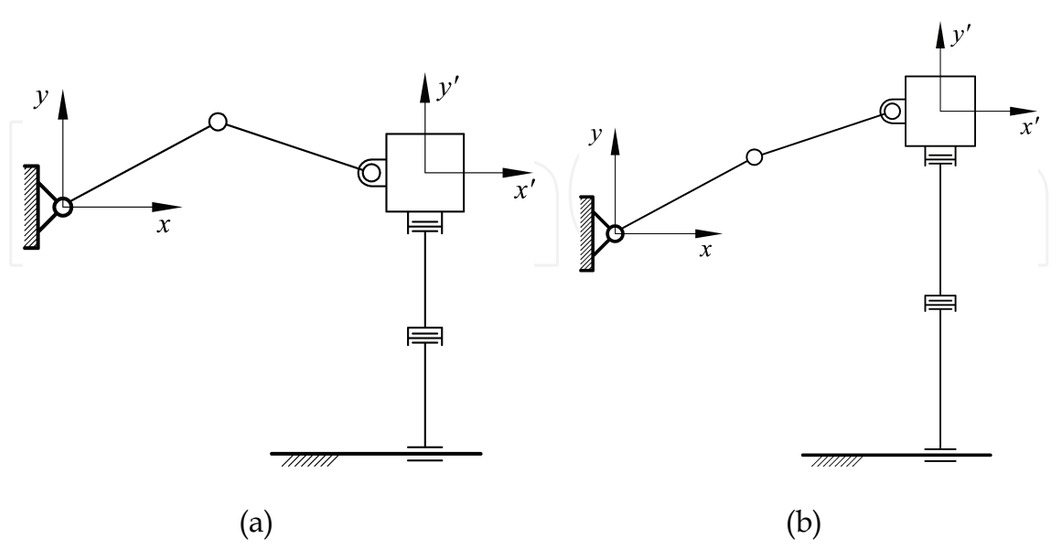

Figure 5. Two kinds of assembly modes: (a) *down-configuration*; (b) *up-configuration*

4. Singularity Analysis

4.1 Jocabian matrix

Equations (6) and (9) can be differentiated with respect to time to obtain the velocity equations. This leads to

$$\dot{s} = \dot{x} \tag{13}$$

$$R_1\left[y\cos\theta - (x - R_3)\sin\theta\right]\dot{\theta} = (x - R_3 - R_1\cos\theta)\dot{x} + (y - R_1\sin\theta)\dot{y} \tag{14}$$

which can be written in an equation of the form

$$\boldsymbol{A}\dot{\boldsymbol{q}} = \boldsymbol{B}\dot{\boldsymbol{p}} \tag{15}$$

where $\dot{\boldsymbol{q}} = \begin{pmatrix}\dot{s} & \dot{\theta}\end{pmatrix}^{\mathrm{T}}$ and $\dot{\boldsymbol{p}} = \begin{pmatrix}\dot{x} & \dot{y}\end{pmatrix}^{\mathrm{T}}$ are the joint and Cartesian space velocity vectors, respectively, and $\boldsymbol{A}$ and $\boldsymbol{B}$ are , respectively, the 2×2 matrices and can be expressed as

$$\boldsymbol{A} = \begin{bmatrix} 1 & 0 \\ 0 & R_1 y\cos\theta - R_1(x - R_3)\sin\theta \end{bmatrix}, \text{ and } \boldsymbol{B} = \begin{bmatrix} 1 & 0 \\ x - R_3 - R_1\cos\theta & y - R_1\sin\theta \end{bmatrix} \tag{16}$$

If matrix $\boldsymbol{A}$ is nonsingular, the Jacobian matrix of the robot can be obtained as

$$\boldsymbol{J} = \boldsymbol{A}^{-1}\boldsymbol{B} = \begin{bmatrix} 1 & 0 \\ \dfrac{x - R_3 - R_1\cos\theta}{R_1 y\cos\theta - R_1(x - R_3)\sin\theta} & \dfrac{y - R_1\sin\theta}{R_1 y\cos\theta - R_1(x - R_3)\sin\theta} \end{bmatrix} \tag{17}$$

from which one can see that there is no any parameter of L_n (n=1,2,3) in this matrix.

4.2 Singularity

In the parallel robot, singularities occur whenever $\boldsymbol{A}$, $\boldsymbol{B}$ or both, become singular. As a singularity leads to an instantaneous change of the robot's DOF, the analysis of parallel robots has drawn considerable attention. For the parallel robot studied here, since there is no any parameter of the leg 2 involved in the Jacobian matrix (see Eqs. (16) and (17)), the singularity is actually only that of the leg 1.

The stationary singularity occurs when $\boldsymbol{A}$ becomes singular but $\boldsymbol{B}$ remains invertible. $|\boldsymbol{A}| = 0$ leads to $R_1 y\cos\theta - R_1(x - R_3)\sin\theta = 0$, i.e. $\tan\theta = y/(x - R_3)$.

Physically, this corresponds to the configuration when leg 1 $A_1B_1P_1$ is completely extended or folded. This singularity is also referred to as the serial singularity. For example, for the robot with the parameters $R_1 = 1.2\text{mm}$ and $R_2 = 0.8\text{mm}$, two configurations of this kind of singularity are shown in Fig. 6. The loci of point P for this kind of singularity can be expressed as

$$C_{fir\_o}: (x - R_3)^2 + y^2 = (R_1 + R_2)^2 \tag{18}$$

and

$$C_{fir\_i}: (x - R_3)^2 + y^2 = (R_1 - R_2)^2 \tag{19}$$

For the above example, if $R_3 = 0.5\text{mm}$ the loci of point P are shown in Fig. 7.
Note that, $R_1 = 0$ leads to $\det(\boldsymbol{A}) = 0$ as well. Therefore, $R_1 = 0$ also results in this kind of singularity.
The uncertainty singularity, occurring only in closed kinematics chains, arises when $\boldsymbol{B}$ becomes singular but $\boldsymbol{A}$ remains invertible. $|\boldsymbol{B}| = 0$ results in $y = R_1 \sin\theta$. Physically, this corresponds to the configuration when link B_1P_1 is parallel to the *x*-axis. Two such configurations are shown in Fig. 8. In such a singularity, the loci of point P can be written as

$$C_{\text{sec}\_r}: (x - R_3 - R_2)^2 + y^2 = {R_1}^2 \tag{20}$$

and

$$C_{\text{sec}\_l}: (x - R_3 + R_2)^2 + y^2 = {R_1}^2 \tag{21}$$

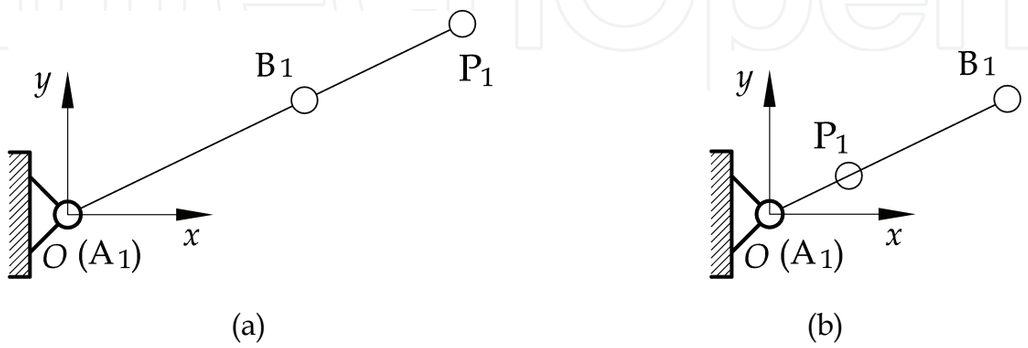

Figure 6. Two kinds configurations of the stationary singularity: (a) $A_1B_1P_1$ is completely extended; (b) $A_1B_1P_1$ is completely folded

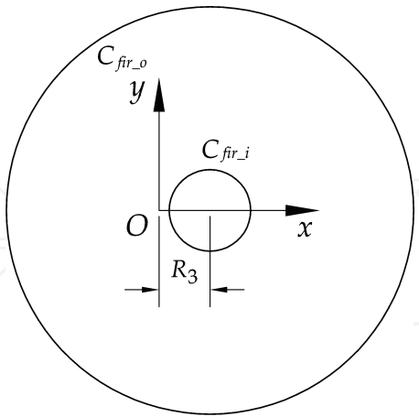

Figure 7. Singular loci of point P when the robot is in the stationary singularity

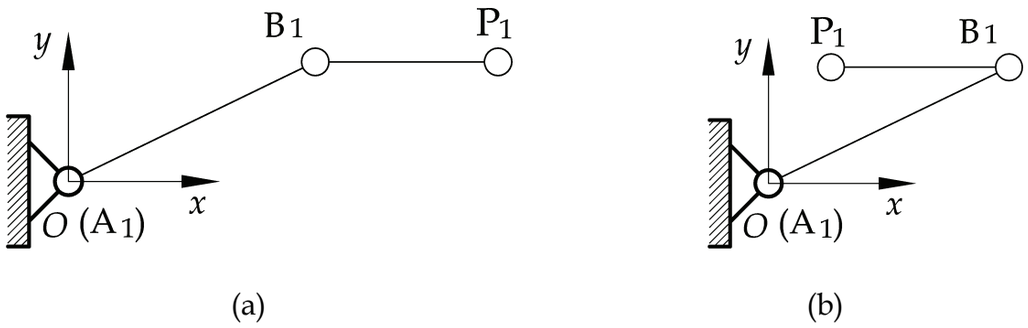

Figure 8. Two kinds configurations of the uncertainty singularity: (a) point P_1 is in the right of point B_1; (b) point P_1 is in the left of point B_1

It is noteworthy that the singular loci of a robot when R_1 is greater than R_2 is different from those when R_2 is greater than R_1. The two cases are shown in Fig. 9. From Figs. 7 and 9, we can see that the uncertainty singular loci are always inside the region bounded by the stationary singular loci; and there are usually tangent points between the two kinds of loci.

The analysis on the kinematics of the robot shows that there are two solutions for both the inverse and forward kinematics. Any one of the singularities will result in the change of solution number of the kinematics. For example, the stationary singularity leads to the loss of solution number of the inverse kinematics. While in the uncertainty singular configuration, the solution number of the forward kinematics can be less or more than two. Then the stationary singularity can be called the inverse kinematic singularity, and the uncertainty singularity the forward kinematic singularity.

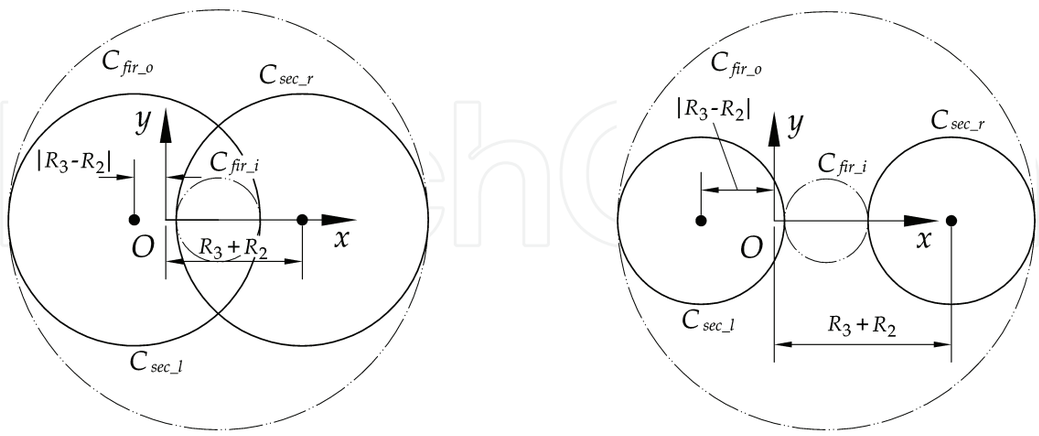

Figure 9. Singular loci of point P when the robot is in the stationary singularity: (a) $R_1 \geq R_2$; (b) $R_1 < R_2$

5. Workspace Analysis

One of the most important issues in the design process of a robot is its workspace. For parallel robots, this issue may be more critical since parallel robots will sometimes have rather a limited workspace.

5.1 Theoretical workspace

Theoretical workspace of the studied robot is defined as the region that the output point can reach if θ changes from 0 to 2π and s between $-\infty$ and ∞ without the consideration of interference between links and the singularity.
From Eq. (6), one can see that if θ is specified, the workspace of the leg 1 is a circle centered at the point $(R_1\cos\theta + R_3,\ \ R_1\sin\theta)$ with a radius of R_2. The circle is denoted as C_{11}. If θ_i changes from 0 to 2π, the center point is located at a circle centered at point $(R_3 \quad 0)$ with a radius of R_1. The circle is denoted as C_{12}. Then, the workspace of the leg is the enveloping region of the circle C_{11} when its center rolls at the circle C_{12}. Actually, the enveloping region is an annulus bounded by two circles C_{fir_o} and C_{fir_i} given in Eqs. (18) and (19), respectively. Especially, when $R_1 = R_2$ the workspace is the region bounded by the circle C_{fir_o}.
Thinking about the architecture of the studied parallel robot, we can see that the workspace of leg 1 is limited with respect to the parameters R_1 and R_2.

But, the workspace of leg 2 has the advantage along *x*-axis. That means the workspace can be infinite if the input *s* is not limited. Practically, this case cannot occur. However, to enlarge the workspace of the robot, we are sure to find a solution that the workspace of leg 1 can be embodied by that of leg 2. Actually, enlarging the workspace is our pursuing objective. In this sense, the workspace of the robot should be that of the leg 1. The workspace of the leg 1 is then our research objective.

For example, the theoretical workspace of leg 1 of the robot with parameters $R_1 = 1.2\text{mm}$, $R_2 = 0.8\text{mm}$ and $R_3 = 0.5\text{mm}$ is shown as the shaded region in Fig. 10. The theoretical workspace and any other type of workspace of the robot can be that which embodies the corresponding workspace of the leg 1 by assigning appropriate values to the parameters L_n (n=1,2,3), which will be described in details in the section 7.2. Therefore, in this chapter, the workspace of the leg 1 is regarded as the workspace of the parallel robot. The theoretical workspace is actually bounded by the stationary singularity loci C_{fir_i} and C_{fir_o}. Its area can be calculated by

$$S_{tw} = \pi\left[(R_1 + R_2)^2 - (R_1 - R_2)^2\right] = 4\pi R_1 R_2 \tag{21}$$

From Fig. 9, we can see that within the theoretical workspace there is stationary singularity.

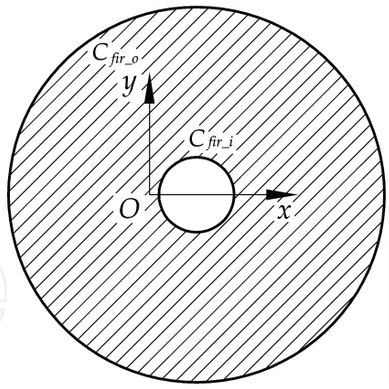

Figure 10. Theoretical workspace of the robot

5.2 Usable workspace

As there exist singular loci inside the theoretical workspace, if a robot wants to move from one point to another it maybe should passes a singular configuration. That means it maybe changes from one working mode to another. In practice, changing working mode during the working process is definitely impossible. Therefore, we should find out a working space without singularity.

The *usable workspace* is defined as the maximum continuous workspace that contains no singular loci inside but bounded by singular loci outside. According to this definition, not every point within the usable workspace can be available for a practical robot. The robot will be out of control at the points on the boundaries and their neighborhoods. But within this region, the robot with a specified working mode can move freely.

In Section 4.2, two kinds of singular loci have been presented for the robot as shown in Fig. 9. The stationary singularity is actually the boundary of a theoretical workspace. Then, a robot with every working mode can have such singular loci. However, as the uncertainty singularity occurs inside the workspace, not every working mode has all such singularities. Normally, for most parallel robots studied here, there are four tangent points between the two kinds of singular loci. The points can be used to identify which singular loci a specified working mode can have. For example, all singular loci of the robot $R_1 = 1.2\text{mm}$, $R_2 = 0.8\text{mm}$ and $R_3 = 0.5\text{mm}$ are shown in Fig. 9. Fig. 11 shows some singular configurations and singular loci of the robot. As shown in Fig. 11, there are four tangent points m, v, q and k between the four singular loci C_{fir_i}, C_{fir_o}, C_{sec_l} and C_{sec_r}. At these four points, both of the stationary and uncertainty singularities occur. The four points divide the singular curves C_{sec_l} and C_{sec_r} into four parts. At the arcs $m1q$ and $v3k$, the robot is in singular only when it is with the "+" mode. At the arcs $m2q$ and $v4k$, the working mode "–" is in singular.

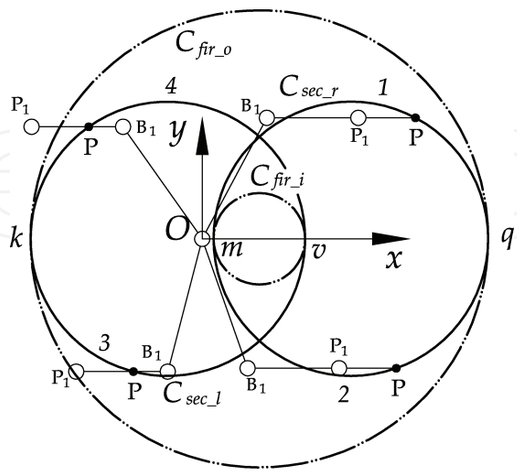

Figure 11. The uncertainty singular loci of a robot with different working modes

What we are concerned about here is the robot with the "+" working mode. Fig. 12 shows all singular loci of such kinds of robots.

The theoretical workspace is divided into two parts by the singular loci shown in Fig. 12, which can be used to identify the usable workspaces of the robots with the "+" working mode and, at the same time, the *down-configuration*. In order to reduce the occupating space, the lower region shown in Fig. 12 is referred to as the *usable workspace* of the parallel robot. They are shown as the shaded region in Fig. 13. Actually, the *usable workspace* is the half of the theoretical workspace. The area can be calculated by

$$S_{uw} = \frac{\pi}{2}\left[(R_1 + R_2)^2 - (R_1 - R_2)^2\right] = 2\pi R_1 R_2 \tag{22}$$

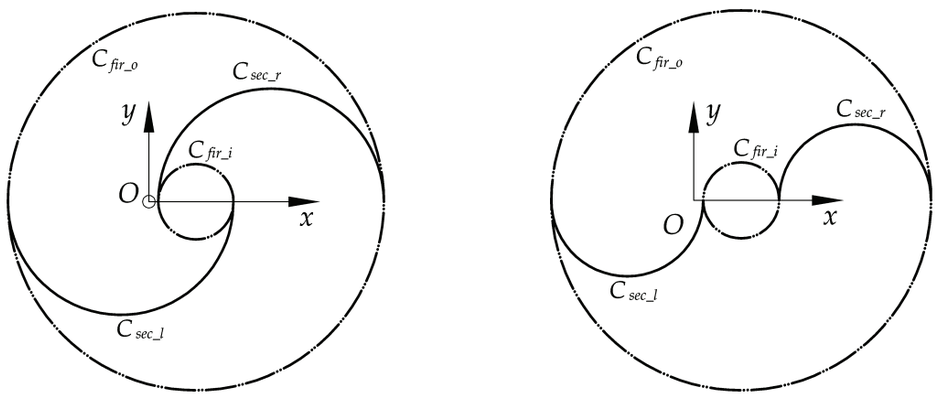

Figure 12. Singular loci of the robot with the "+" working mode: (a) $R_1 \geq R_2$; (b) $R_1 < R_2$

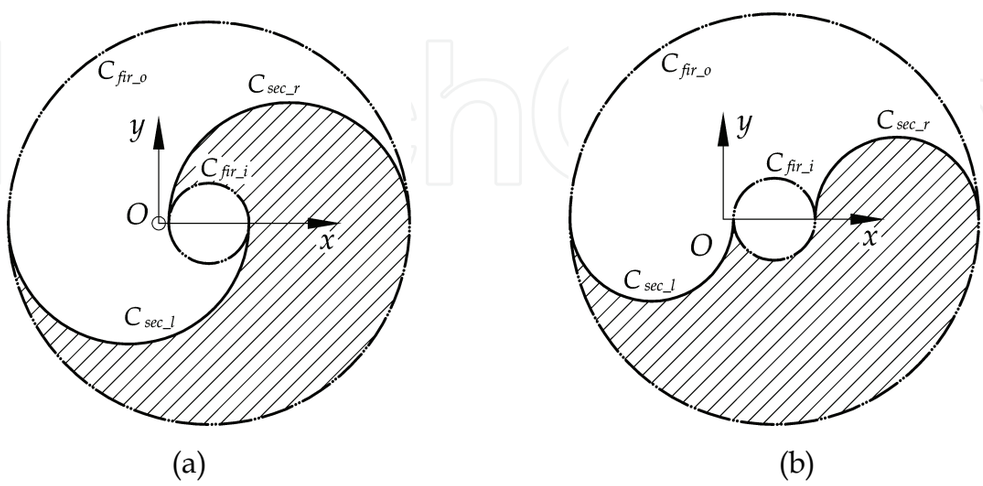

Figure 13. Usable workspace of the robot with both the "+" working mode and *down-configuration*: (a) $R_1 \geq R_2$; (b) $R_1 < R_2$

5.3 Workspace atlas

To apply a specified robot in practice, we usually should determine the link lengths with respect to a desired application. This is actually the so-called optimal kinematic design (parameter synthesis) of the robot. In such a process, one of the most classical tools that has been using is the chart.
Chart is a kind of tool to show the relationship between concerned parameters. As it is well known, the performance of a parallel robot depends not only on the pose of the end-effector but also on the link lengths (dimensions). Disregarding the pose, each of the links can be the length between zero and infinite. And there are always several links in a parallel robot. Then the combination of the links with different lengths will be infinite. They undoubtedly have different performance characteristics. In order to summarize the characteristics of a performance, we must show the relationship between it and geometrical parameters of the parallel robot. To this end, a finite space that must contain all kinds of robots (with different link lengths) should be first developed. Next is to plot the chart considering a desired performance. In this paper, the space is referred to as the design space. The chart that can show the relationship between performances and link lengths is referred to as atlas.

5.3.1 Development of a design space

The Jacobian matrix is the matrix that maps the relationship between the velocity of the end-effector and the vector of actuated joint rates. This matrix is the most important parameter in the field. Almost all performances are depended on this parameter. Therefore, based on the Jacobian matrix, we can identify which geometrical parameter should be involved in the analysis and kinematic design.
For the parallel robot considered here, there are three parameters in the Jacobian matrix (see Eq. (17)), which are R_1, R_2 and R_3. Theoretically, any one of the parameters R_1, R_2 and R_3 can have any value between zero and infinite. This is the biggest difficulty to develop a design space that can embody all robots (with different link lengths) within a finite space. For this reason, we must eliminate the physical link size of the robots.

Let

$$D = (R_1 + R_2 + R_3)/3 \tag{23}$$

One can obtain 3 non-dimensional parameters r_i by means of

$$r_1 = R_1/D,\ r_2 = R_2/D,\ r_3 = R_3/D \tag{24}$$

This would then yield

$$r_1 + r_2 + r_3 = 3 \tag{25}$$

From Eq.(25), the three non-dimensional parameters r_1, r_2 and r_3 have limits, i.e.,

$$0 < r_1,\ r_2,\ r_3 < 3 \tag{26}$$

Based on Eqs. (25) and (26), one can establish a design space as shown in Fig. 14(a), in which the triangle ABC is actually the design space of the parallel robot. In Fig. 14(a), the triangle ABC is restricted by r_1, r_2 and r_3. Therefore it can be figured in another form as shown in Fig. 14(b), which is referred to as the planar-closed configuration of the design space. In this design space, each point corresponds a kind of robot with specified value of r_1, r_2 and r_3.

For convenience, two orthogonal coordinates r and t are utilized to express r_1, r_2 and r_3. Thus, by using

$$\begin{cases} r = 2r_1/\sqrt{3} + r_3/\sqrt{3} \\ t = r_3 \end{cases} \tag{27}$$

coordinates r_1, r_2 and r_3 can be transformed into r and t. Eq. (27) is useful for constructing a performance atlas.

From the analysis of singularity and workspace, we can see that the singular loci and workspace shape of a robot when $r_1 > r_2$ are different from those of the robot when $r_1 < r_2$. For the convenience of analysis, the line $r_1 = r_2$ is used to divide the design space into two regions as shown in Fig. 14(b).

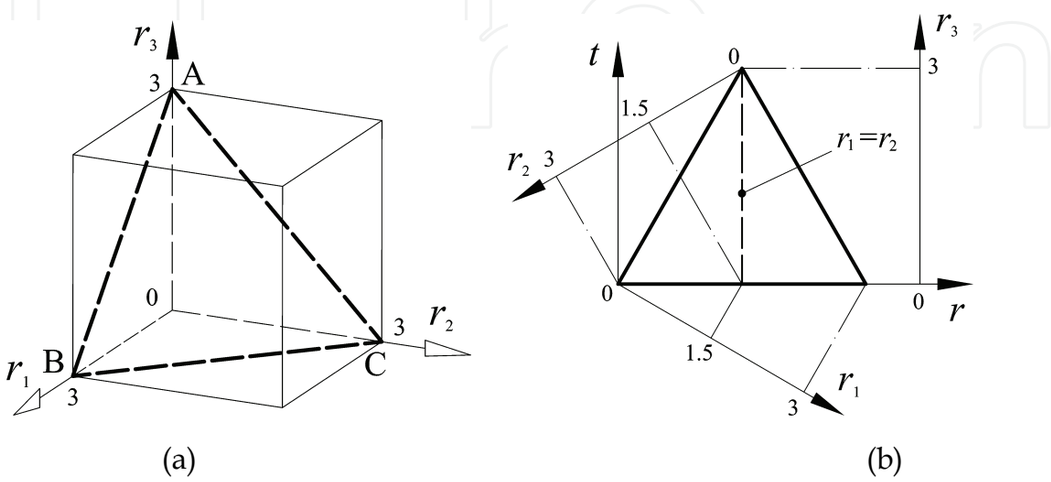

Figure 14. Design space of the 2-DOF translational parallel robot

5.3.2 Workspace characteristics

Using the normalization technique in Eqs. (23) and (24), the dimensional parameters R_1, R_2 and R_3 were changed to non-dimensional ones r_1, r_2 and r_3. The kinematic, singularity and workspace analysis results can be obtained by replacing R_n (n=1,2,3) with r_n (n=1,2,3) in Eqs. (2)-(22). Then, using Eq. (21), we can calculate the theoretical workspace area of each robot in the design space shown in Fig. 14(b). As a result, the atlas of the workspace can be plotted as shown in Fig. 15. To plot the atlas, one should first calculate the theoretical workspace area of each non-dimensional robot with r_1, r_2 and r_3, which is included in the design space. Using the Eq. (27), one can then obtain the relationship between the area and the two orthogonal coordinates r and t (see Fig. 14(b)). This relationship is practically used to plot the atlas in the planar system with r and t. The subsequent atlases are also plotted using the same method. Fig. 15 shows not only the relationship between the workspace area and the two orthogonal coordinates but that between the area and the three non-dimensional parameters as well. What we are really most concerned about is the later relationship. For this reason, r and t are not appeared in the figure. From Fig. 15, one can see that

- The theoretical workspace area is inverse proportional to parameter r_3;
- The area atlas is symmetric with respect to $r_1 = r_2$, which means that the area of a kind of robot with $r_1 = u$, $r_2 = w$ $(u, w < 3)$ and $r_3 = 3 - u - w$ is identical to that of a robot with $r_1 = w$, $r_2 = u$ $(u, w < 3)$ and $r_3 = 3 - u - w$;
- The area reaches its maximum value when $r_1 = r_2 = 1.5$ and $r_3 = 0$. The maximum value is 9π.

Since the *usable workspace* area is the half of the theoretical workspace area, the atlas of *usable workspace* is identical with that of Fig. 15 in distribution but is different in area value. From Figs. 10 and 15, we can see that the theoretical workspaces of robots $r_1 = u$ and $r_2 = w$, and $r_1 = w$ and $r_2 = u$ are identical with each other not only in area but also in shape. It is noteworthy that, although, the *usable workspace* area atlas is also symmetric about the line $r_1 = r_2$, the *usable workspace* shape of the robot with $r_1 = u$ and $r_2 = w$ is no longer same as that of the robot with $r_1 = w$ and $r_2 = u$. This result is not difficult to be reached from Fig. 13.

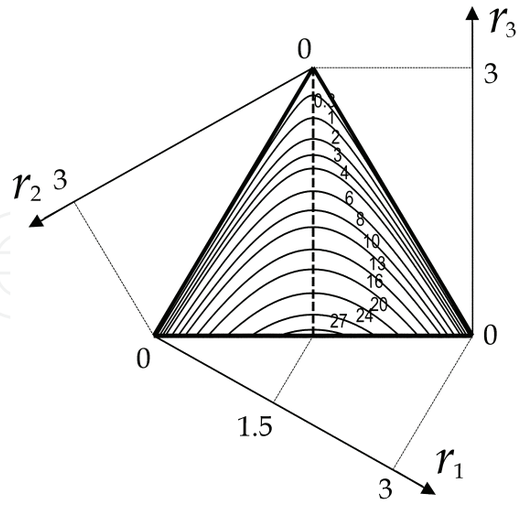

Figure 15. Atlas of the theoretical workspace of the parallel robot

5.3.3 Similarity robots

From Fig. 15, one can know the workspace performance of a non-dimensional parallel robot. Our objective is usually the dimensional robot. If the workspace performance of a robot with parameters r_n (n=1,2,3) is clear, one should know the corresponding performance of the robot with parameters R_n (n=1,2,3). Otherwise, the normalization of geometric parameters and the developed design space will be nonsense. Comparing Eqs. (21) and (22), it is not difficult to reach the following relationship

$$S_{tw} = D^2 S'_{tw} \text{ and } S_{uw} = D^2 S'_{uw} \tag{28}$$

where S'_{tw} and S'_{uw} are the theoretical and usable workspace areas, respectively, of a non-dimensional robot. Eq. (28) indicates that the workspace of a dimensional robot is D^2 times that of a non-dimensional robot. That means, from Fig. 15, one can also know the workspace performance of a dimensional robot.

Therefore, the robot with normalized parameters rn (n=1,2,3) has a generalized significance. The workspace performance of such a robot indicates not only the performance of itself but also those of the robots with parameters Drn, i.e. Rn. Here, the robots with parameters Drn are defined as similarity robots; and the robot with parameters rn is referred to as the basic similarity robot. The analysis in the subsequent sections will show that the similarity robots are similar in terms of not only the workspace performance but also other performances, such as conditioning index and stiffness. For these reasons, the normalization of the geometric parameters can be reasonably applied to the optimal design of the robot. And it also simplifies the optimal design process.

6. Atlases of Good-Condition Indices

From Section 5, one can know characteristics of the workspace, especially the usable workspace of a robot with given r_n or R_n (n=1,2,3). Usually, in the design process and globally evaluation of a performance, a kind of workspace is inevitable. Unfortunately, due to the singularity, neither the theoretical workspace nor the *usable workspace* can be used for these purposes. Therefore, we should define a workspace where each configuration of the robot can be far away from the singularity. As it is well known, the condition number of Jacobian matrix is an index to measure the distance of a configuration to the singularity. The local conditioning index, which is the reciprocal of the condition number, will then be used to define some good-condition indices in this section.

6.1 Local conditioning index

Mathematically, the condition number of a matrix is used in numerical analysis to estimate the error generated in the solution of a linear system of equations by the error in the data (Strang, 1976). The condition number of the Jacobian matrix can be written as

$$\kappa = \left\| \boldsymbol{J} \right\| \left\| \boldsymbol{J}^{-1} \right\| \tag{29}$$

where $\left\| \bullet \right\|$ denotes the Euclidean norm of the matrix, which is defined as

$$\left\| \boldsymbol{J} \right\| = \sqrt{tr\left(\boldsymbol{J}^T \boldsymbol{W} \boldsymbol{J} \right)}; \quad \boldsymbol{W} = \frac{1}{n} \boldsymbol{I} \tag{30}$$

in which n is the dimension of the Jacobian matrix and $\boldsymbol{I}$ the $n \times n$ identity matrix. Moreover, one has

$$1 \le \kappa \le \infty \tag{31}$$

and hence, the reciprocal of the condition number, i.e., $1/\kappa$, is always defined as the local conditioning index (LCI) to evaluate the control accuracy, dexterity and isotropy of a robot. This number must be kept as large as possible. If the number can be unity, the matrix is an isotropic one, and the robot is in an isotropic configuration.

6.2 Good-condition workspace

Let's first check how the LCI is at every point in the workspace of the similarity robot with parameters $R_1 = 1.2\text{mm}$, $R_2 = 0.8\text{mm}$ and $R_3 = 0.5\text{mm}$. Its *us-*

able workspace is shown in Fig. 13(a). Fig. 16 shows the distribution of the LCI in the workspace.

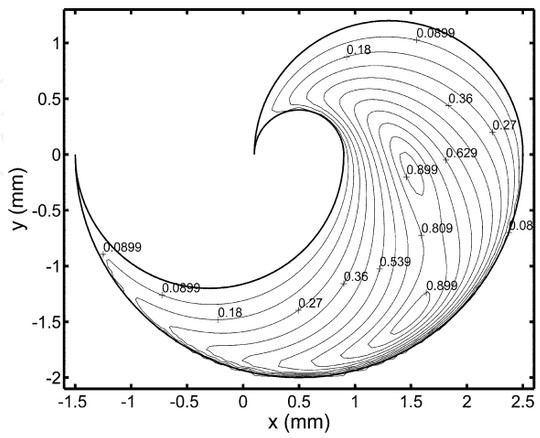

Figure 16. Distribution of the LCI in the usable workspace

From Fig. 16 one can see that, in the *usable workspace*, there exist some points where the LCI will be zero or very small. At these points the control accuracy of the robot will be very poor. These points will not be used in practice. They should be excluded in the design process. The left workspace, which will be used in practice, can be referred to as good-condition workspace (GCW) that is bounded by a specified LCI value, i.e., $1/\kappa$. Then, the set of points where the LCI is greater than or equal to (GE) a specified LCI is defined as the GCW.
Using the numerical method, by letting the minimum LCI be 0.3, the GCW area of each basic similarity robot in the design space shown in Fig. 14(b) can be calculated.

The corresponding atlas can be then plotted as shown in Fig. 17, from which one can see that

- The GCW area is inverse proportional to parameter r_3;
- The area atlas is no longer symmetric with respect to the line $r_1 = r_2$. In another sense, this indicates that a large theoretical or usable workspace of a robot doesn't mean that it has a large GCW;
- The maximum value of the GCW area is still that of the robot $r_1 = r_2 = 1.5$ and $r_3 = 0$.

Since there is no singularity within the whole GCW, it can be used as a reference in the definition of a global index, e.g. global conditioning index.

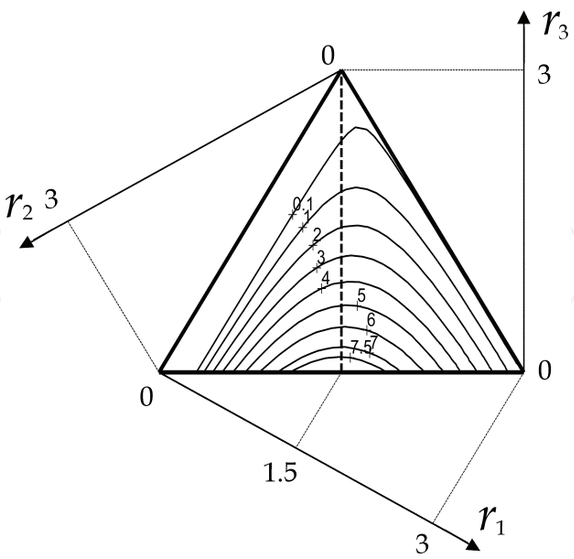

Figure 17. Atlas of the good-condition workspace when LCI ≥ 0.3

6.3 Global conditioning index

Jacobian matrix is pose-dependent (see Eq. (17)). Then, the LCI is depended on the pose as well. This indicates that the LCI at one point may be different from that at another point. Therefore, the LCI is a local index. In order to evaluate the global behaviour of a robot on a workspace, a global index can be defined as (Gosselin & Angeles, 1989)

$$\eta_J = \int_W 1/\kappa_J \, dW \Big/ \int_W dW \tag{32}$$

which is the global conditioning index (GCI). In Eq. (32), W is the workspace. In particular, a large value of the index ensures that a robot can be precisely controlled.

For the robot studied here, the workspace W in Eq. (32) can be the GCW when LCI ≥ 0.3. The relationship between the GCI and the three normalized parameters r_n (n=1,2,3) can be studied in the design space. The corresponding atlas is shown in Fig. 18, from which one can see that the robots near $r_1 = 1.2$ have large GCI. Some of these robots have very large GCW, some very small.

6.4 Global stiffness index

Disregarding the physical characteristic, kinematically, there will be deformation on the end-effector if an external force acts on it.

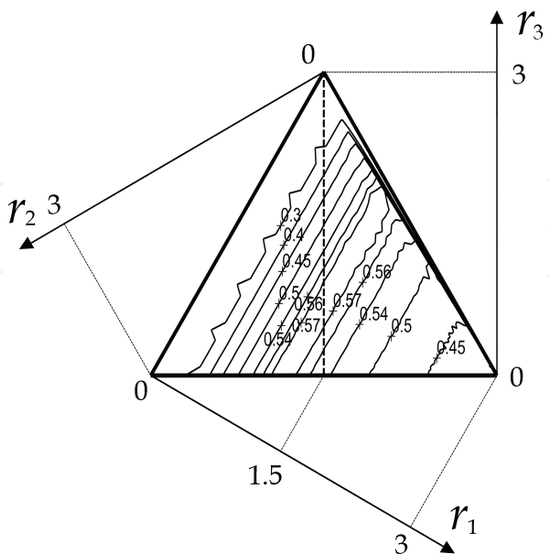

Figure 18. Atlas of the global conditioning index

This deformation is dependent on the robot's stiffness and on the external force. The robot stiffness affects the dynamics and position accuracy of the device, for which stiffness is an important performance index. The static stiffness (or rigidity) of the robot can be a primary consideration in the design of a parallel robot for certain applications.

Equation (8) can be rewritten as

$$\dot{\boldsymbol{q}} = \boldsymbol{J}\dot{\boldsymbol{p}} \tag{33}$$

On the other hand, by virtue of what is called the duality of kinematics and statics (Waldron & Hunt, 1988), the forces and moments applied at the end-effector under static conditions are related to the forces or moments required at the actuators to maintain the equilibrium by the transpose of the Jacobian matrix $\boldsymbol{J}$. We can write

$$\boldsymbol{\tau} = \boldsymbol{J}^{\mathrm{T}} f \tag{34}$$

where f is the vector of actuator forces or torques, and $\boldsymbol{\tau}$ is the generalized vector of Cartesian forces and torques at the end-effector.
In the joint coordinate space, a diagonal stiffness matrix $\boldsymbol{K}_p$ is defined to express the relationship between the actuator forces or torques f and the joint displacement vector $\Delta \boldsymbol{q}$ according to

$$f = K_p \Delta q \tag{35}$$

With

$$K_p = \begin{bmatrix} k_{p1} & \\ & k_{p2} \end{bmatrix} \tag{36}$$

in which k_{pi} is a scalar representing the stiffness of each of the actuators.

In the operational coordinate space, we define a stiffness matrix K which relates the external force vector τ to the output displacement vector D of the end-effector according to

$$\tau = KD \tag{37}$$

The Eq. (33) also describes the relationship between the joint displacement vector Δq and the output displacement vector D, i.e.,

$$\Delta q = JD \tag{38}$$

From Eqs. (34), (35) and (38), we get

$$\tau = J^{\mathrm{T}} K_p J D \tag{39}$$

Thus, the stiffness matrix K is expressed as

$$K = J^{\mathrm{T}} K_p J \tag{40}$$

Then, we have

$$D = K^{-1} \tau \tag{41}$$

From Eq. (41), one can write

$$D^{\mathrm{T}} D = \tau^{\mathrm{T}} \left(K^{-1}\right)^{\mathrm{T}} K^{-1} \tau \tag{42}$$

Let the external force vector τ be unit, i.e.,

$$\|\tau\|^2 = \tau^{\mathrm{T}} \tau = 1 \tag{43}$$

Under the condition (43), one can derive the extremum of the norm of vector $\boldsymbol{D}$. In order to obtain the conditional extremum, using the Lagrange multiplier λ_D, one can construct the Lagrange equation as following

$$L_D = \boldsymbol{\tau}^{\mathrm{T}}\left(\boldsymbol{K}^{-1}\right)^{\mathrm{T}}\boldsymbol{K}^{-1}\boldsymbol{\tau} - \lambda_D\left(\boldsymbol{\tau}^{\mathrm{T}}\boldsymbol{\tau} - 1\right) \tag{44}$$

The necessary condition to the conditional extremum is

$$\frac{\partial L_D}{\partial \lambda_D} = 0:\ \boldsymbol{\tau}^{\mathrm{T}}\boldsymbol{\tau} - 1 = 0, \text{ and } \frac{\partial L_D}{\partial \boldsymbol{\tau}} = 0:\ \left(\boldsymbol{K}^{-1}\right)^{\mathrm{T}}\boldsymbol{K}^{-1}\boldsymbol{\tau} - \lambda_D\,\boldsymbol{\tau} = 0 \tag{45}$$

from which one can see that the Lagrange multiplier λ_D is actually an eigenvalue of the matrix $\left(\boldsymbol{K}^{-1}\right)^{\mathrm{T}}\boldsymbol{K}^{-1}$. Then, the norm of vector $\boldsymbol{D}$ can be written as

$$\|\boldsymbol{D}\|^2 = \boldsymbol{D}^{\mathrm{T}}\boldsymbol{D} = \boldsymbol{\tau}^{\mathrm{T}}\left(\boldsymbol{K}^{-1}\right)^{\mathrm{T}}\boldsymbol{K}^{-1}\boldsymbol{\tau} = \boldsymbol{\tau}^{\mathrm{T}}\,\lambda_D\,\boldsymbol{\tau} = \lambda_D \tag{46}$$

Therefore, the extremum of $\|\boldsymbol{D}\|^2$ is the extremum of the eigenvalues of the matrix $\left(\boldsymbol{K}^{-1}\right)^{\mathrm{T}}\boldsymbol{K}^{-1}$. Then, if $k_{p1} = k_{p2} = 1$ and $\|\boldsymbol{\tau}\|^2 = 1$, the maximum and minimum deformations on the end-effector can be described as

$$\|\boldsymbol{D}_{\max}\| = \sqrt{\max\left(\left|\lambda_{Di}\right|\right)} \text{ and } \|\boldsymbol{D}_{\min}\| = \sqrt{\min\left(\left|\lambda_{Di}\right|\right)} \tag{47}$$

where λ_{Di} $(i = 1,2)$ are the eigenvalues of the matrix $\left(\boldsymbol{K}^{-1}\right)^{\mathrm{T}}\boldsymbol{K}^{-1}$. $\|\boldsymbol{D}_{\max}\|$ and $\|\boldsymbol{D}_{\min}\|$ are actually the maximum and minimum deformations on the end-effector when both the external force vector and the matrix $\boldsymbol{K}_p$ are unity. The maximum and minimum deformations form a deformation ellipsoid, whose axes lie in the directions of the eigenvectors of the matrix $\left(\boldsymbol{K}^{-1}\right)^{\mathrm{T}}\boldsymbol{K}^{-1}$. Its magnitudes are the maximum and minimum deformations given by Eq. (47). The maximum deformation $\|\boldsymbol{D}_{\max}\|$, which can be used to evaluate the stiffness of the robot, is defined as the local stiffness index (LSI). The smaller the deformation is, the better the stiffness is.

Similarly, based on Eq. (47), the global stiffness index (GSI) that can evaluate the stiffness of a robot within the workspace is defined as

$$\eta_{D\max} = \frac{\int_W \|\boldsymbol{D}_{\max}\| dW}{\int_W dW} \tag{48}$$

where, for the robot studied here, W is the GCW when $\mathrm{LCI} \geq 0.3$. Usually, $\eta_{D\max}$ can be used as the criterion to design the robot with respect to its stiffness. Normally, we expect that the index value should be as small as possible. Figure 19 shows the atlas of $\eta_{D\max}$, from which one can see that the larger the parameter r_3, the smaller the deformation. That means the stiffness is proportional to the parameter r_3.

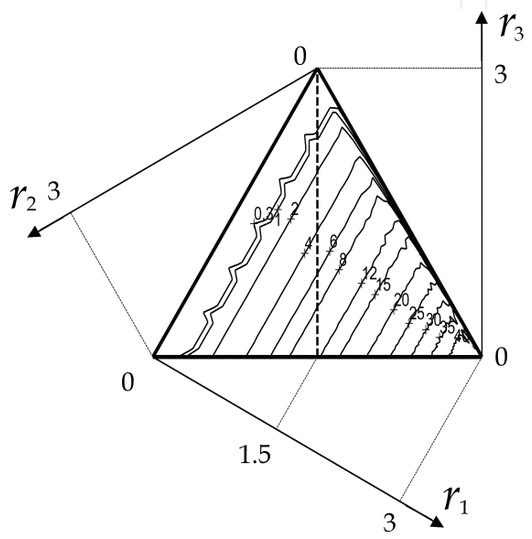

Figure 19. Atlas of the global stiffness index

7. Optimal Design based on the Atlas

In this section, a method for the optimal kinematic design of the parallel robot will be proposed based on the results of last sections.

7.1 Optimum region with respect to desired performances

Relationships between performance indices and the link lengths of the 2-DOF translational parallel robot have been studied. The results have been illustrated by their atlases, from which one knows visually which kind of robot can be with a better performance and which cannot. This is very important for us to find out a global optimum robot for a specified application. In this section, the optimum region will be shown first with respect to possible performances.

7.1.1 Workspace and GCI

In almost all designs, the workspace and GCI are usually considered. From the atlas of the GCW (see the Fig. 17), we can see that the workspace of a robot when r_1 is near 1.5 and r_3 is shorter can be larger. From the atlas of GCI (Fig. 18), we know that robots near $r_1 = 1.2$ have better GCI. If the GCW area, denoted as S'_{GCW}, is supposed to be greater than 6 ($S'_{GCW} > 6$) and the GCI greater than 0.54, the optimum region in the design space can be obtained shown as the shaded region in Fig. 20(a). The region is denoted as $\Omega_{GCW-GCI} = \left[(r_1,\ r_2,\ r_3) \mid S'_{GCW} > 6 \text{ and } \eta_J > 0.54\right]$ with performance restriction. One can also obtain an optimum region with better workspace and GCI, for example, the region $\Omega'_{GCW-GCI}$ where $S'_{GCW} > 7$ and $\eta_J > 0.57$ as shown in Fig. 20(b). In order to get a better result, one can decrease the optimum region with stricter restriction. Such a region contains some *basic similarity robots*, which are all possible optimal results.

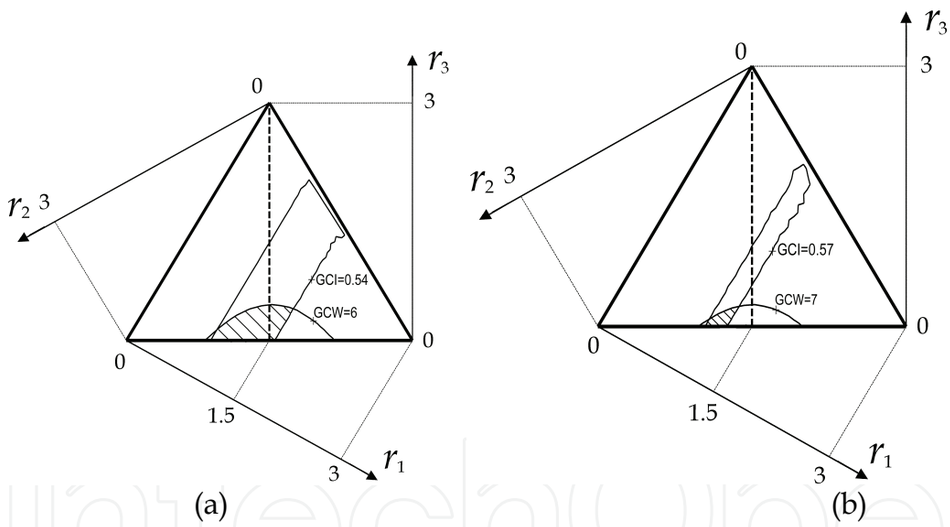

Figure 20. Two optimum region examples with respect to both GCI and GCW performance restrictions

After the optimum region is identified, there are two ways to achieve the optimal design result with non-dimensional parameters. One is to search a most optimal result within the region $\Omega_{GCW-GCI}$ or $\Omega'_{GCW-GCI}$ using one classical searching algorithm based on an established object function. The method will yield a unique solution. This is not the content of this paper. Another one is to select a robot within the obtained optimum region. For example, the *basic similarity robot* with $r_1 = 1.2$, $r_2 = 1.65$ and $r_3 = 0.15$ can be selected as the candidate if only workspace and GCI are involved in the design. Its GCW area and the

GCI value are 7.2879 and 0.5737, respectively. The robot with only r_n (n=1,2,3) parameters and its GCW are shown in Fig. 21.

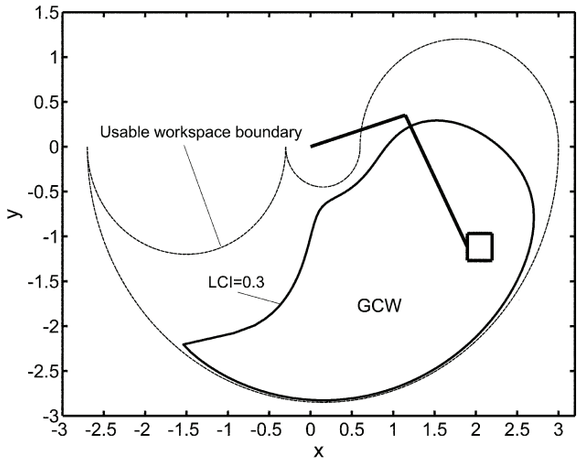

Figure 21. The robot with parameters $r_1 = 1.2$, $r_2 = 1.65$ and $r_3 = 0.15$ in the $\Omega'_{GCW-GCI}$ region and its GCW when LCI ≥ 0.3

Actually, we don't recommend the former method for achieving an optimal result. The solution based on the objective function approach is a mathematical result, which is unique. Such a result is maybe not the optimal solution in practice. Practically, we usually desire a solution subjecting to our application conditions. From this view, it is unreasonable to provide a unique solution for the optimal design of a robot. Since we cannot predict any application condition previously, it is most ideally to provide all possible optimal solutions, which allows a designer to adjust the link lengths with respect to his own design condition. The advantage of the later method is just such an approach that allows the designer to adjust the design result fitly by trying to select another candidate in the optimum region.

7.1.2 Workspace, GCI, and GSI

In this paper, stiffness is evaluated by the maximum deformation of the end-effector when the external force and the stiffness of each of the actuators are unit. A robot with smaller $\eta_{D\max}$ value usually has better stiffness. Since accuracy is inherently related to the stiffness, actually, the stiffness index used here can also evaluate the accuracy of the robot. To achieve an optimum region with respect to all of the three indices, the GCW can be specified as $S'_{GCW} > 6$, GCI $\eta_J > 0.54$ and GSI $\eta_{D\max} < 7.0$. The optimal region will be $\Omega_{GCW-GCI-GSI} = \lfloor (r_1,\ r_2,\ r_3) \mid S'_{GCW} > 6,\ \eta_J > 0.54,\ \text{and}\ \eta_{D\max} < 7 \rceil$ shown in Fig. 22. For

example, the values of the GCW, GCI and GSI of the *basic similarity robot* with parameters $r_1 = 1.12$, $r_2 = 1.68$ and $r_3 = 0.2$ in the optimum region are $S'_{GCW} = 6.8648$, $\eta_I > 0.5753$ and $\eta_{D\max} = 6.5482$. Fig. 23 shows the robot and its GCW when LCI is GE 0.3.

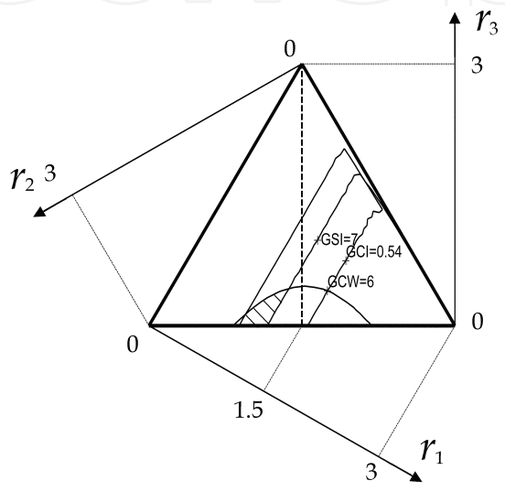

Figure 22. One optimum region example with respect to the GCI, GCW and GSI performance restrictions

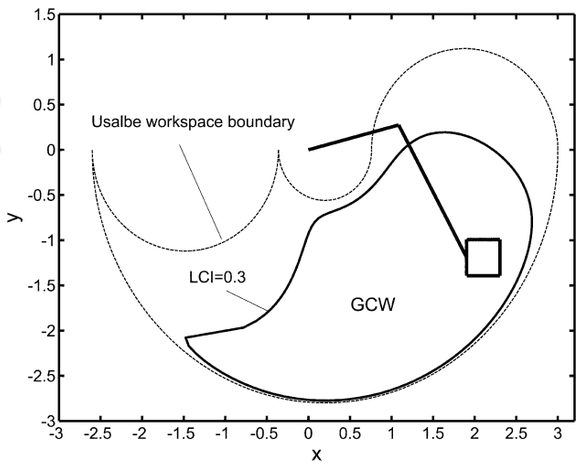

Figure 23. The robot with parameters $r_1 = 1.12$, $r_2 = 1.68$ and $r_3 = 0.2$ in the $\Omega_{GCW-GCI-GSI}$ region and its GCW when LCI ≥ 0.3

7.2 Dimension determination based on the obtained optimum example

The final objective of optimum design is determining the link lengths of a robot, i.e. the *similarity robot*. In the last section, some optimum regions have been presented as examples. These regions consist of *basic similarity robots* with non-dimensional parameters. The selected optimal *basic similarity robots* are comparative results, not final results. Their workspaces may be too small to be used in practice. In this section, the dimension of an optimal robot will be determined with respect to a desired workspace.

As an example of presenting how to determine the *similarity robot* with respect to the optimal *basic similarity robot* obtained in section 7.1, we consider the robot with parameters $r_1 = 1.12$, $r_2 = 1.68$ and $r_3 = 0.2$ selected in section 7.1.2. The robot is from the optimum region $\Omega_{GCW-GCI-GSI}$, where the workspace, GCI and stiffness are all involved in the design objective. To improve the GCI and GSI performances of the robot, letting LCI be GE 0.5, the values of the GCW, GCI and GSI of the robot with parameters $r_1 = 1.12$, $r_2 = 1.68$ and $r_3 = 0.2$ are $S'_{GCW} = 4.0735$, $\eta_J > 0.6977$ and $\eta_{D\max} = 2.5373$. Fig. 24 shows the revised GCW. Comparing Figs. 23 and 24, it is obvious that the improvement of performances GCI and GSI is based on the sacrifice of the workspace area.

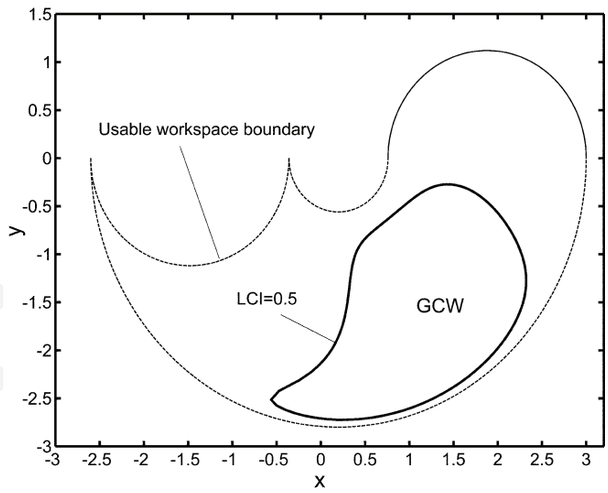

Figure 24. GCW of the robot with parameters $r_1 = 1.12$, $r_2 = 1.68$ and $r_3 = 0.2$ when $\mathrm{LCI} \geq 0.5$

The process to find the dimensions with respect to a desired practical workspace can be summarized as following:

Step 1: Investigating the distribution of LCI and LSI on the GCW of the *basic similarity robot*. For the aforementioned example, the distribution is

shown in Fig. 25 (a) and (b), respectively, from which one can see the distributing characteristics of the two performances. The investigation can help us determining whether it is necessary to adjust the GCW. For example, if the stiffness at the worst region of the GCW cannot satisfy the specification on stiffness, one can increase the specified LCI value to reduce the GCW. In contrary, if the stiffness is permissible, one can decrease the specified LCI value to increase the GCW.

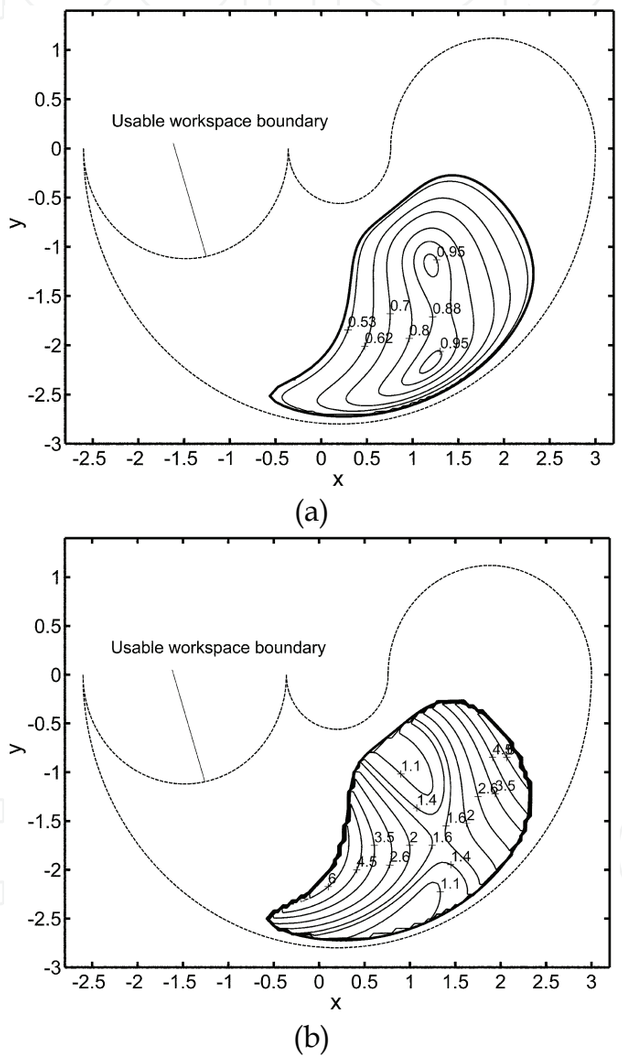

Figure 25. Distribution of LCI and LSI in the GCW of the *basic similarity robot* when LCI≥0.5: (a) LCI; (b) LSI

Step 2: Determining the factor D, which was used to normalize the parameters of a dimensional robot to those that are non-dimensional. The GCW area when LCI≥0.5 of the selected *basic similarity robot* is

$S'_{GCW} = 4.0735$. If the desired workspace area S_{GCW} of a dimensional robot is given with respect to the design specification, the factor D can be obtained as $D = \sqrt{S_{GCW}/S'_{GCW}}$, which is identical with the relationship in Eq. (28). For example, if the desired workspace shape is similar to the GCW shown in Fig. 24 and its area $S_{GCW} = 500\text{mm}$, there is $D = \sqrt{S_{GCW}/S'_{GCW}} = \sqrt{500/4.0735} \approx 11.08\text{mm}$.

Step 3: Achieving the corresponding *similarity robot* by means of dimensional factor D. As given in Eq. (24), the relationship between a dimensional parameter and a non-dimensional one is $R_n = Dr_n$ (n=1,2,3). Then, if D is determined, R_n can be obtained. For the above example, there are $R_1 = 12.41\text{mm}$, $R_2 = 18.61\text{mm}$ and $R_3 = 2.22\text{mm}$. In this step, one can also check the performances of the *similarity robot*. For example, Fig. 26 (a) shows the distribution of LCI on the desired workspace, from which one can see that the distribution is the same as that shown in Fig. 25 (a) of the *basic similarity robot*. The GCI is still equal to 0.6977. Fig. 26 (b) illustrates the distribution of LSI on the workspace. Comparing Fig. 26 (b) with Fig. 25 (b), one can see that the distributions of LSI are the same. The GSI value is still equal to 2.5373. Then, the factor D does not change the GCI, GSI, and the distributions of LCI and LSI on the workspaces. For such a reason, we can say that, if a *basic similarity robot* is optimal, any one of its *similarity robots* is optimal.

Step 4: Determining the parameters L_n (n=1,2,3) that are relative to the leg 2. Since the parameters are not enclosed in the Jacobian matrix, they are not the optimized objects. They can be determined with respect to the desired workspace. Strictly speaking, the workspace analyzed in the former sections is that of the leg 1. As mentioned in section 5.1, to maximize the workspace of the 2-DOF parallel translational robot and, at the same time, to reduce the cost, the parameters L_n (n=1,2,3) should be designed as those with which the workspace of leg 2 can just embody the workspace of the leg 1. To this end, the parameters should be subject to the following equations

$$Y_{\max} = L_1 + L_2 - L_3 + R_3 \tag{49}$$

$$Y_{\min} = L_1 - L_2 - L_3 + R_3 \tag{50}$$

in which $Y_{\max}$ and $Y_{\min}$ are *y*-coordinates of the topmost and lowest points of the desired workspace. For the desired GCW shown in Fig. 26, there are $Y_{\max} = \text{-}3.32\text{mm}$ and $Y_{\min} = \text{-}29.92\text{mm}$. Substituting them

in Eqs. (49) and (50), we have $L_2 = 13.30\text{mm}$. To reduce the manufacturing cost, let $L_1 = L_2$, which leads to $L_3 = 32.14\text{mm}$

Step 5: Calculating the input limit for each actuator. The range of each input parameter can be calculated from the inverse kinematics. For the obtained *similarity robot*, there are $\theta \in [-83.3040°,\ 81.7649°]$ and $s \in [-6.10\text{mm},\ 25.49\text{mm}]$.

Then, the parameters of the optimal robot with respect to the desired workspace $S_{GCW} = 500\text{mm}$ are $R_1 = 12.41\text{mm}$, $R_2 = 18.61\text{mm}$, $R_3 = 2.22\text{mm}$, $L_1 = L_2 = 13.30\text{mm}$, $L_3 = 32.14\text{mm}$, $\theta \in [-83.3040°,\ 81.7649°]$ and $s \in [-6.10\text{mm},\ 25.49\text{mm}]$. It is noteworthy that this result is only one of all possible solutions. If the designer picks up another *basic similarity robot* from the optimum region, the final result will be different. This is actually one of the advantages of this optimal design method. The designer can adjust the final result to fit his design condition. It is also worth notice that, actually, the desired workspace shape cannot be that shown in Fig. 26. It is usually in a regular shape, for example, a circle, a square or a rectangle. In this case, a corresponding similar workspace should be first identified in the GCW of the *basic similarity robot* in **Step 2**. This workspace, which is the subset of the GCW, is normally just embodied by the GCW. The identified workspace area will be used to determine the factor *D* with respect the desired workspace area in **Step 2**.

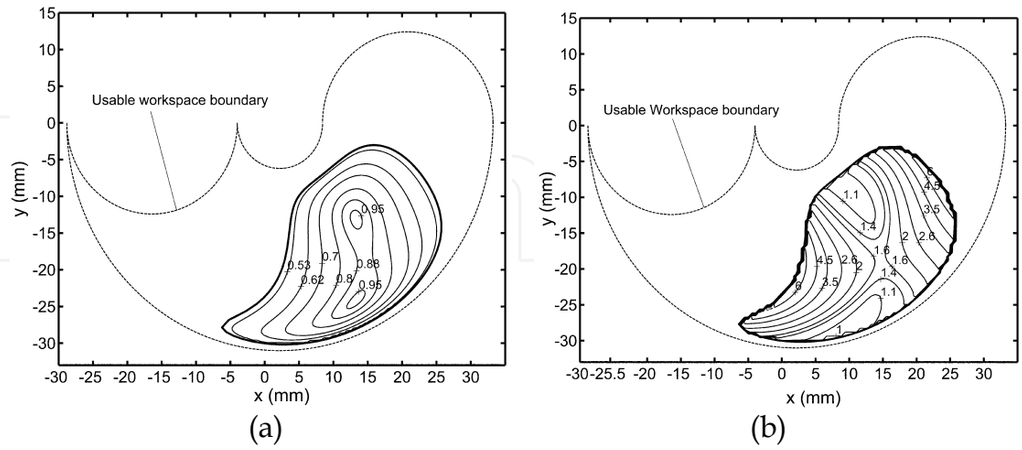

(a) (b)

Figure 26. Distribution of LCI and LSI in the desired workspace of the obtained *similarity robot*: (a) LCI; (b) LSI

8. Conclusion and Future Works

In this chapter, a novel 2-DoF translational robot is proposed. One advantage of the robot is that it can position a rigid body in a 2D plane while maintaining a constant orientation. The proposed robot can be used in light industry where high speed is needed. The inverse and forward kinematics problems, workspace, conditioning indices, and singularity are presented here. In particular, the optimal kinematic design of the robot is investigated and a design method is proposed.

The key issue of this design method is the construction of a geometric design space based on the geometric parameters involved, which can embody all *basic similarity robots*. Then, atlases of desired indices can be plotted. These atlases can be used to identify an optimal region, from which an ideal candidate can be selected. The real-dimensional parameters of a *similarity robot* can be found by considering the desired workspace and the *good-condition workspace* of the selected *basic similarity robot*. Compared with other design methods, the proposed methodology has some advantages: (a) one performance criterion corresponds to one atlas, which can show visually and globally the relationship between the index and design parameters; (b) for the same reason in (a), the fact that some performance criteria are antagonistic is no longer a problem in the design; (c) the optimal design process can consider multi-objective functions or multi-criteria, and also guarantees the optimality of the result; and finally, (d) the method provides not just one solution but all possible solutions.

The future work will focus on the development of the computer-aided design of the robot based on the proposed design methodology, the development of the robot prototype, and the experience research of the prototype.

Acknowledgement

This work was supported by the National Natural Science Foundation of China (No. 50505023), and partly by Tsinghua Basic Research Foundation.

9. References

Asada, H. and Kanade, T. (1983). Desgin of direct-drive mechanical arms, *ASME Journal of Vibration, Acoustics, Stress, and Reliability in Design,* Vol.105, pp.312-316.

Bonev, I. (2001). The Delta parallel robot-the story of success, http://www.parallelmic. org/Reviews/Review002p.html.

Carricato, M. and Parenti-Castelli, V. (2001). A family of 3-DOF translational parallel manipulators, *Proceedings of the 2001 ASME Design Engineering*

Technical Conferences, Pittsburgh, Pennsylvania, paper DETC2001/DAC-21035.

Cervantes-Sánchez, J.J., Hernández-Rodríguez, J.C. and Angeles, J. (2001) On the kinematic design of the 5R planar, symmetric manipulator, *Mechanism and Machine Theory*, Vol.36, pp.1301-1313

Chablat, D. & Wenger, P. (2003). Architecture optimization of a 3-DoF parallel mechanism for machining applications: the Orthoglide, IEEE Transactions on Robotics and Automation, Vol. 19, pp.403–410

Clavel, R. (1988). DELTA: a fast robot with parallel geometry, *Proceedings of 18th Int. Symp. on Industrial Robot*, pp. 91-100.

Gao, F., Liu, X.-J. and Gruver, W.A. (1998). Performance evaluation of two degrees of freedom planar parallel robots, *Mechanisms and Machine Theory*, Vol.33, pp.661-668.

Gosselin, C. & Angeles, J. (1989). The optimum kinematic design of a spherical three-degree-of-freedom parallel manipulator, *J. Mech. Transm. Autom. Des.*, Vol.111, pp.202-207

Gosselin, C.M. & Angeles, J. (1990). Singularity analysis of closed loop kinematic chains, *IEEE Trans. on Robotics and Automation,* Vol.6, pp.281-290.

Gough, V. E. (1956). Contribution to discussion of papers on research in automobile stability, control and tyre performance, *Proceedings of Auto Div Inst Mech Eng*, pp.392-395.

Hervé, J. M. (1992). Group mathematics and parallel link mechanisms, *Proceedings of IMACS/SICE Int. Symp. On Robotics, Mechatronics, and Manufacturing Systems*, pp.459-464.

Hunt, K. H. (1978). *Kinematic geometry of mechanisms*, Clarendon Press, Oxford.

Kim, H.S. & Tsai, L.-W. (2002). Design optimization of a Cartesian parallel manipulator, *Proceedings of ASME 2002 Design Engineering Technical Conferences and Computers and Information in Engineering Conference*, Montreal, Canada, paper DETC2002/MECH-34301

Kong, X. & Gosselin, C.M. (2002). Kinematics and singularity analysis of a novel type of 3-CRR 3-DOF translational parallel manipulator, *International Journal of Robotics Research*, Vol.21, pp.791-798.

Liu, X.-J. (2001). *Mechanical and kinematics design of parallel robotic mechanisms with less than six degrees of freedom*, Post-Doctoral Research Report, Tsinghua University, Beijing.

Liu, X.-J. & Kim, J. (2005). A new spatial three-DoF parallel manipulator with high rotational capability, *IEEE/ASME Transactions on Mechatronics*, Vol.10, No.5, pp.502-512.

Liu, X.-J. & Wang, J. (2003). Some new parallel mechanisms containing the planar four-bar parallelogram, *International Journal of Robotics Research*, Vol.22, No.9, pp.717-732

Liu, X.-J., Jeong, J., & Kim, J. (2003). A three translational DoFs parallel cube-manipulator, *Robotica*, Vol.21, No.6, pp.645-653.

Liu, X.-J., Kim, J. and Wang, J. (2002). Two novel parallel mechanisms with less than six DOFs and the applications, *Proceedings of Workshop on Fundamental Issues and Future Research Directions for Parallel Mechanisms and Manipulators*, pp. 172-177, Quebec City, QC, Canada, October, 2002.

Liu, X.-J., Wang, J., Gao F., & Wang, L.-P. (2001). On the analysis of a new spatial three degrees of freedom parallel manipulator, *IEEE Transactions on Robotics and Automation*, Vol.17, pp.959-968.

Liu, X.-J., Wang, Q.-M., & Wang, J. (2005). Kinematics, dynamics and dimensional synthesis of a novel 2-DOF translational manipulator, *Journal of Intelligent & Robotic Systems*, Vol.41, No.4, pp.205-224.

McCloy, D. (1990). Some comparisons of serial-driven and parallel driven mechanisms, *Robotica*, Vol.8, pp.355-362.

Merlet, J.-P. (2000). *Parallel robots*, Kluwer Academic Publishers, London.

Ottaviano, E. & Ceccarelli, M. (2002). Optimal design of CaPaMan (Cassino Parallel Manipulator) with a specified orientation workspace, *Robotica*, Vol.20, pp.159–166

Siciliano, B. (1999). The Tricept robot: inverse kinematics, manipulability analysis and closed- loop direct kinematics algorithm, *Robotica,* Vol.17, pp.437-445.

Stewart, D. (1965). A platform with six degrees of freedom, *Proc Inst Mech Eng*, Vol.180, pp.371-386,

Stock, M. & Miller, K. (2004). Optimal kinematic design of spatial parallel manipulators: application to linear Delta robot, *Journal of Mechanical Design*, Vol.125, pp.292-301

Strang, G. (1976). *Linear algebra and its application*, Academic Press, New York

Tonshoff, H.K., Grendel, H. and Kaak, R. (1999). Structure and characteristics of the hybrid manipulator Georg V, In: *Parallel Kinematic Machines*, C.R. Boer, L. Molinari- Tosatti and K.S. Smith (editors), pp.365-376, Springer-Verlag London Limited.

Tsai, L. W. & Stamper, R. (1996). A parallel manipulator with only translational degrees of freedom, *Proceedings of ASME 1996 Design Engineering Technical Conference*, Irvine, CA, paper 96-DETC-MECH -1152.

Waldron, K.J. & Hunt, K.H. (1988). Series-parallel dualities in actively coordinated mechanisms, *Robotics Research*, Vol.4, pp.175-181.

Zhao, T. S. & Huang, Z. (2000). A novel three-DOF translational platform mechanism and its kinematics, *Proceedings of ASME 2000 International Design Engineering Technical Conferences*, Baltimore, Maryland, paper DETC2000/MECH-14101.

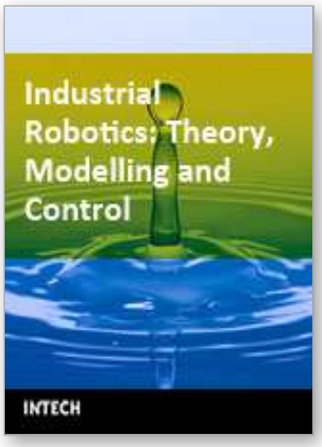

Industrial Robotics: Theory, Modelling and Control

Edited by Sam Cubero

ISBN 3-86611-285-8

Hard cover, 964 pages

Publisher Pro Literatur Verlag, Germany / ARS, Austria

Published online 01, December, 2006

Published in print edition December, 2006

This book covers a wide range of topics relating to advanced industrial robotics, sensors and automation technologies. Although being highly technical and complex in nature, the papers presented in this book represent some of the latest cutting edge technologies and advancements in industrial robotics technology. This book covers topics such as networking, properties of manipulators, forward and inverse robot arm kinematics, motion path-planning, machine vision and many other practical topics too numerous to list here. The authors and editor of this book wish to inspire people, especially young ones, to get involved with robotic and mechatronic engineering technology and to develop new and exciting practical applications, perhaps using the ideas and concepts presented herein.

InTech Europe
University Campus STeP Ri
Slavka Krautzeka 83/A
51000 Rijeka, Croatia
Phone: +385 (51) 770 447
Fax: +385 (51) 686 166
www.intechopen.com

InTech China
Unit 405, Office Block, Hotel Equatorial Shanghai
No.65, Yan An Road (West), Shanghai, 200040, China
中国上海市延安西路65号上海国际贵都大饭店办公楼405单元
Phone: +86-21-62489820
Fax: +86-21-62489821

IntechOpen